Available online at www.sciencedirect.com
ScienceDirect
Journal of Power Sources 177 (2008) 579–589
JOURNAL OF POWER SOURCES
www.elsevier.com/locate/jpowsour

Modeling and simulation of solid oxide fuel cell based on the volume–resistance characteristic modeling technique

Lijin Wang, Huisheng Zhang *, Shilie Weng

The Key Laboratory of Power Machinery and Engineering of Education Ministry, Shanghai Jiao Tong University, Shanghai 200240, PR China

Received 2 September 2007; received in revised form 18 October 2007; accepted 18 October 2007
Available online 24 October 2007

Abstract

Solid oxide fuel cell (SOFC) is a complicated system with heat and mass transfer as well as electrochemical reactions. The real-time dynamic simulation of SOFC is still a challenge up to now. This paper develops a one-dimensional mathematical model for direct internal reforming solid oxide fuel cell (DIR-SOFC). The volume–resistance (*V–R*) characteristic modeling technique is introduced into the modeling of the SOFC system. Based on the *V–R* modeling technique and the modular modeling idea, ordinary differential equations meeting the quick simulation are obtained from partial differential equations. This model takes into account the variation of local gas properties. It can not only reflect the distributed parameter characteristics of SOFC, but also meet the requirement of the real-time dynamic simulation. The results indicate that the *V–R* characteristic modeling technique is valuable and viable in the SOFC system, and the model can be used in the quick dynamic and real-time simulation.

Keywords: Solid oxide fuel cell (SOFC); Volume–resistance characteristic modeling technique; Distributed and lumped parameter; Dynamic simulation

1. Introduction

Solid oxide fuel cells (SOFCs) are energy conversion devices that produce electricity and heat directly from a gaseous or gasified fuel by electrochemical reaction with an oxidant [1]. SOFC operates at high temperature and atmospheric or higher pressure, and can use hydrogen, carbon monoxide, and hydrocarbons as fuel, and air or pure oxygen as oxidant. As a matter of fact, both simple-cycle and hybrid SOFC systems have been demonstrated among the highest efficiencies of any power generation system, combined with minimal air pollutant emissions and low greenhouse gas emissions. These capabilities have made SOFC an attractive emerging technology for stationary power generation, especially for the distributed generation [2].

The conventional modeling technique for a distributed parameter SOFC is to establish a set of partial differential equations based on the conservation equations for species mass, total mass, momentum and energy. The solution to these equation sets is very difficult and very time consuming. In addition, sometimes the exact numerical solution may be impossible. However, the SOFC dynamic and real-time simulation is of significance in the verification of controller or online monitoring system. In order to overcome this problem and also provide reference for optimization design of the SOFC, we need a real-time model which is also a time saving model.

The main purposes of this paper are as following: first, considering the variation of local flow properties, such as pressure, mass flow rate, density, specific heat capacity, thermal conductivity and dynamic viscosity; secondly, introducing the volume–resistance characteristic modeling technique into the SOFC system to establish a modular model satisfying the quick dynamic simulation; finally, developing a dynamic model of a planar DIR-SOFC cell.

2. SOFC mathematical model

There have been several publications focusing on modeling the performance of SOFCs. Such models can be for different geometries, PEN (positive-electrode/electrolyte/negative-electrode) structures, flow configurations, and operating temperature ranges, etc. [1,3–20]. Most publications have been addressed based on CFD with detailed parameters or steady and

* Corresponding author. Tel.: +86 21 34206823; fax: +86 21 34206103.
E-mail address: zhslm@sjtu.edu.cn (H. Zhang).

0378-7753/$ – see front matter © 2007 Elsevier B.V. All rights reserved.
doi:10.1016/j.jpowsour.2007.10.051

Nomenclature

A_j	cross-section area of the channel (m^2)
C_p	specific heat capacity ($kJ\,kg^{-1}\,K^{-1}$)
d_h	hydraulic diameter (m)
e	specific internal energy ($kJ\,kg^{-1}$)
f	resistance coefficient
F	Faraday constant (C) or molar flow rate ($mol\,s^{-1}$)
G	mass flow rate ($kg\,s^{-1}$)
h_j	height of the channel (m)
H	specific enthalpy ($kJ\,kg^{-1}$)
I, $\bar{I}$	local and average current density ($A\,m^{-2}$)
$k_{i,PEN}$, $k_{i,INTC}$	air and fuel channels heat transfer coefficient ($kJ\,m^{-1}\,s^{-1}\,K^{-1}$)
L	width of the activation area of the fuel cell (m)
LHV	lower heating value ($kJ\,mol^{-1}$)
P	pressure (Pa) or power density ($W\,m^{-2}$)
p	partial pressure (Pa)
R	gas constant ($J\,mol^{-1}\,K^{-1}$)
u_j	velocity in gas channels ($m\,s^{-1}$)
U	voltage (V) or utilization
W	width of the activation area of the fuel cell (m)
y_i	molar fraction of component i

Greek letters

ΔH	enthalpy change of reaction ($kJ\,mol^{-1}$)
η	fuel electrical efficiency
λ_a, λ_f	thermal conductivity of the air and fuel steam ($kJ\,m^{-1}\,s^{-1}\,K^{-1}$)
λ_{PEN}, λ_{INTC}	thermal conductivity of PEN and interconnector ($kJ\,m^{-1}\,s^{-1}\,K^{-1}$)
μ	dynamic viscosity
$v_{i,k}$	stoichiometric coefficient of component i in reaction k
ρ	density of gas steams and solid parts ($kg\,m^{-3}$)
σ	Stefan–Boltzmann constant 5.676E−8 ($W\,m^{-2}\,K^{-4}$)
σ_{anode}, $\sigma_{cathode}$	electronic conductivity of anode and cathode ($\Omega^{-1}\,m^{-1}$)
$\sigma_{electrolyte}$	ionic conductivity of electrolyte ($\Omega^{-1}\,m^{-1}$)
τ	thickness of solid structures (m)
$\in$	emissivity

Subscripts

a	air channel
anode	anode polar
cathode	cathode polar
electrolyte	electrolyte
f	fuel channel
INTC	interconnector
ocp	open circuit potential
PEN	PEN structure

Superscripts

in	fuel and air inlet

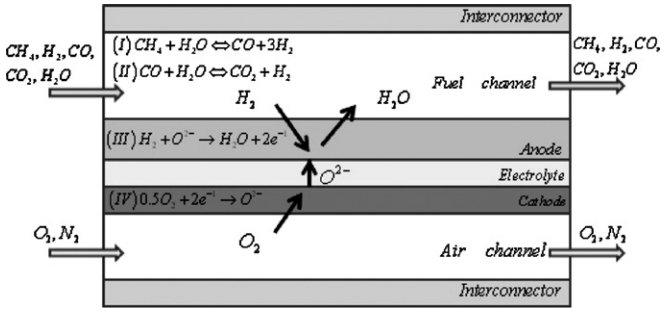

Fig. 1. Schematic principle view of a co-flow planar SOFC cell.

dynamic model with many assumptions and simplifications, for example the flow properties and gas velocity are taken as constant throughout the system based on the inlet conditions. In recent years, several papers (Iora et al. [3], Janardhanan et al. [19], Liu et al. [20]) have considered the variation of local gas properties. But owing to the complicated numerical iteration, these models could not meet the requirement of the real-time dynamic simulation.

The dynamic SOFC model developed here, which is one-dimensional planar DIR-SOFC model, considers the variation of local flow properties, and allows for co-flow and counter-flow operations. The approach to avoid the iteration of the coupling of pressure and mass flow rate is based on the volume–resistance characteristic modeling technique, the distributed–lumped parameter method and the modular modeling idea. The established model can not only reflect the characteristics of distributed parameter, but also satisfy the requirement of the transient simulation. Fig. 1 presents the schematic principle view of a co-flow planar DIR-SOFC cell.

To simplify the modeling, some reasonable assumptions are summarized as follows:

(1) Only H_2 is electrochemically oxidized.
(2) Constant Nusselt number.
(3) Adiabatic boundaries for the cell.

2.1. Species mass balances model

The chemical species considered in the fuel channel are CH_4, H_2, CO, CO_2 and H_2O, while in the air channel the chemical species are O_2 and N_2 (as the oxidant is considered to be air and not pure oxygen). In Table 1 the reactions and the corresponding reaction rates in the SOFC system are presented. It is assumed all CO is converted through the water gas shift reaction (II), which is at equilibrium; all CH_4 in the fuel is only concerned with the steam reforming reaction (I). The molar flux in both gas channels is considered convective in the flow direction. It is reasonable to neglect the axial dispersion effects [1]. The detailed gas properties (density, specific heat capacity, thermal conductivity, dynamic viscosity, etc.) are mainly affected by the local temperature and the components, their detailed calculations can be found in the references [22,23]. For instance, the dynamic viscosity of multi-component gas mixtures is based on the Reichenberg's expression, and the thermal conductivity

Table 1
Reactions and reaction rates in the SOFC system

Steam reforming [1,4,5]	(I)$CH_4 + H_2O \Leftrightarrow CO + 3H_2$	$R_{(I)} = k_{act} p_{f,CH_4} \exp\left(-\frac{E_{act}}{RT_f}\right)$	(1)
Water gas shift [1,4]	(II)$CO + H_2O \Leftrightarrow CO_2 + H_2$	$R_{(II)} = k_{WGSR} p_{f,CO}\left(1 - \frac{p_{f,CO_2} p_{f,H_2}}{k_{shift} p_{f,CO} p_{f,H_2O}}\right)$	(2)
Oxidation Reduction	(III)$H_2 + O^{2-} \rightarrow H_2O + 2e^{-1}$ (IV)$0.5O_2 + 2e^{-1} \rightarrow O^{2-}$	$R_{(III,IV)} = \frac{I}{2F}$	(3)

Table 2
Species mass balances equations of SOFC model

Fuel channel : $$\frac{\partial C_{f,i}}{\partial t} = -\frac{\partial C_{f,i} u_f}{\partial x} + \sum_{k \in \{(I),(II),(III)\}} v_{i,k} R_k \frac{1}{h_f}, \quad i \in \{CH_4, H_2, CO, CO_2, H_2O\} \quad (4)$$

Air channel : $$\frac{\partial C_{a,i}}{\partial t} = -\frac{\partial C_{a,i} u_a}{\partial x} + v_{i,(IV)} R_{(IV)} \frac{1}{h_a}, \quad i \in \{O_2, N_2\} \quad (5)$$

of multi-component gas mixtures is based on the Wassiljewa's expression and the Mason and Saxena modification (Poling et al. [23]).

The kinetics of the reforming reaction (I), the water gas shift reaction (II) and the electrochemical reaction (III), which are listed in Table 1. The first order kinetic expression derived by Achenbach and Riensche [5] has been adopted in the reforming reaction (I), with an activation energy of $E_{act} = 82 \times 10^3\ J\ mol^{-1}$ and a pre-exponential constant of $k_{act} = 0.04274\ mol\ s^{-1}\ m^{-2}\ Pa^{-1}$. Such formation is considered typically for the DIR-SOFC performance [1]. The water gas shift reaction (II) is considered a very fast one and is assumed to be at equilibrium in the fuel channel [6]. The equilibrium limited shift reaction rate expression is derived by Aguiar et al. [1], where $k_{shift} = \exp(4276/T_f - 3.961)$ [7]. The kinetic of the electrochemical reaction is only related to the local electric current density.

The detailed species mass balances equations listed in Table 2 are referred to the literature [3].

2.2. Mass balances model

For the mass balance, oxygen ions produced in the cathode transfer to the PEN structure. Hydrogen in the fuel channel will penetrate into the PEN structure as well, where the electrochemical reaction occurs. The water steam produced from the reaction transfers to the fuel channel. Therefore the increased mass in the fuel channel is only owing to the mass transfer of the oxygen ions. For the whole system the mass is conserved. The detailed Eqs. (6) and (7) are listed in Table 3, where v_{O_2} is stoichiometric coefficient of oxygen, R_{O_2} the oxygen reaction rate, in fact it is the same to the electrochemical reaction rate, and M_{O_2} is the oxygen molecular weight.

Table 3
Mass balances equations of SOFC model

Fuel channel : $$\frac{\partial \rho_f}{\partial t} = -\frac{\partial \rho_f u_f}{\partial x} - v_{O_2} R_{O_2} M_{O_2} \frac{1}{h_f} \quad (6)$$

Air channel : $$\frac{\partial \rho_a}{\partial t} = -\frac{\partial \rho_a u_a}{\partial x} + v_{O_2} R_{O_2} M_{O_2} \frac{1}{h_a} \quad (7)$$

2.3. Energy balances model

In a SOFC system, current and temperature distributions are strongly coupled. Therefore, exact energy balances model and accurate temperature profiles in the fuel cell are very important and essential. The model in Table 4 considers that the thermal flux in both the PEN structure and interconnector is conductive, which is modeled by Fourier's law of heat conduction. Meanwhile, the thermal flux in the gas channels is convective from the gas channels to the solid parts [1]. The heat transfer coefficients between the gas channels and the solid parts were calculated using a constant Nusselt number (here, it is taken to be 3.09; Aguiar et al. [1]). In general, an assumption is given for the laminar flow conditions that the Nusselt number is considered independent of the Reynolds number [24]. Due to the high temperatures involved, radiation energy between the PEN structure and interconnector is also included.

Here, the following enthalpy change in every reaction is derived according to the method depicted detailed in the reference [25], where ΔH° is the enthalpy change at the standard state:

$$\Delta H_I = \Delta H^\circ{}_I - 16373.61 + R\left(7.951T_f - 4.354e - 3T_f^2 + 0.7213e - 6T_f^3 - \frac{0.097e5}{T_f}\right) \quad (14)$$

$$\Delta H_{II} = \Delta H^\circ{}_{II} - 7756.56 + R\left(1.86T_f - 0.27e - 3T_f^2 + \frac{1.164e5}{T_f}\right) \quad (15)$$

$$\Delta H_{III} = \Delta H^\circ{}_{III} + 4097.22 + R\left(-1.5985T_{PEN} + 0.3875e - 3T_{PEN}^2 - \frac{0.1515e5}{T_{PEN}}\right) \quad (16)$$

2.4. Momentum balances model

To calculate the pressure profiles in the fuel and air channels, a momentum balance for each gas channel is required. The energy conservational equations of Iora et al. [3] revised a little are adopted, which are presented in Table 5.

Table 4
Energy balances equations of SOFC model

Fuel channel

$$\frac{\partial(\rho_f e_f)}{\partial t} = -\frac{\partial(\rho u_f C_{p,f} T_f)}{\partial x} + \left[k_{f,PEN}(T_{PEN} - T_f) + k_{f,INTC}(T_{INTC} - T_f) + \sum_{k\in[(I),(II)]} (-\Delta H)_k R_k\right]\frac{1}{h_f} \quad (8)$$

$$e_f = H_f - \frac{P_f}{\rho_f} \quad (9)$$

Air channel

$$\frac{\partial(\rho_a e_a)}{\partial t} = -\frac{\partial(\rho_a u_a C_{p,a} T_a)}{\partial x} + [k_{a,PEN}(T_{PEN} - T_a) + k_{a,INTC}(T_{INTC} - T_a)]\frac{1}{h_a} \quad (10)$$

$$e_a = H_a - \frac{P_a}{\rho_a} \quad (11)$$

PEN structure

$$\frac{\partial T_{PEN}}{\partial t} = \frac{\lambda_{PEN}}{\rho_{PEN} C_{p,PEN}} \times \frac{\partial^2 T_{PEN}}{\partial x^2} - \frac{1}{\rho_{PEN} C_{p,PEN} \tau_{PEN}} \left\{k_{f,PEN}(T_{PEN} - T_f) + k_{a,PEN}(T_{PEN} - T_a) - [(-\Delta H)_{(IV)} R_{(IV)} - I \cdot U] - \left[\frac{\sigma(T_{INTC}^4 - T_{PEN}^4)}{1/\in_{INTC} + 1/\in_{PEN} - 1}\right]\right\} \quad (12)$$

Interconnector

$$\frac{\partial T_{INTC}}{\partial t} = \frac{\lambda_{INTC}}{\rho_{INTC} C_{p,INTC}} \times \frac{\partial^2 T_{INTC}}{\partial x^2} - \frac{1}{\rho_{INTC} C_{p,INTC} \tau_{INTC}} \left\{k_{f,INTC}(T_{INTC} - T_f) + k_{a,INTC}(T_{INTC} - T_a) + \left[\frac{\sigma(T_{INTC}^4 - T_{PEN}^4)}{1/\in_{INTC} + 1/\in_{PEN} - 1}\right]\right\} \quad (13)$$

Table 5
Momentum balances equations of SOFC model

$$\text{Fuel channel}: \frac{\partial \rho_f u_f}{\partial t} = -\frac{\partial \rho_f u_f u_f}{\partial x} - \frac{\partial P_f}{\partial x} - \frac{2f(W, h_f)\cdot u_f \mu_f}{d^2} \quad (17)$$

$$\text{Air channel}: \frac{\partial \rho_a u_a}{\partial t} = -\frac{\partial \rho_a u_a u_a}{\partial x} - \frac{\partial P_a}{\partial x} - \frac{2f(W, h_a)\cdot u_a \mu_a}{d^2} \quad (18)$$

2.5. Electrochemical model

The electrochemical model here considers the distribution parameter. The open circuit potential U_{ocp} is determined by the gas composition in both gas channels and local temperature at the PEN structure. It is depicted by the Nernst equation as follows:

$$U_{ocp} = U_{H_2}^0 + \frac{RT_{PEN}}{2F}\ln\left(\frac{p_{f,H_2}(p_{a,O_2})^{0.5}}{p_{f,H_2O}}\right) + \frac{RT_{PEN}}{4F}\ln\left(\frac{1}{P_{std}}\right) \quad (19)$$

where

$$U_{H_2}^0 = 1.2723 - 2.7645e-4 \times T_{PEN} \quad (20)$$

$U_{H_2}^0$ is the ideal voltage for hydrogen oxidization [2,8]. P_{std} is taken as the standard pressure.

Only activation and ohmic losses are taken into account, and concentration loss is neglected [1]. Ohmic resistances are caused by resistance to conduction of ions and electrons and contact resistance between cell components [1,9,10,11]:

$$R_{ohm} = \frac{\tau_{anode}}{\sigma_{anode}} + \frac{\tau_{electrolyte}}{\sigma_{electrolyte}} + \frac{\tau_{cathode}}{\sigma_{cathode}} \quad (21)$$

Overpotentials at the cathode and at the anode are assumed independent of the local current density. The model derived by Achenbach [6] is adopted, where activation energies $E_{anode} = 110\,kJ\,mol^{-1}$, $E_{cathode} = 160\,kJ\,mol^{-1}$, and corresponding coefficients $k_{anode} = 2.13E{+}8\,A\,m^{-2}$, $k_{cathode} = 1.49E{+}10\,A\,m^{-2}$, $m = 0.25$:

$$\frac{1}{R_{anode}} = k_{anode}\frac{2F}{RT_f}\left(\frac{p_{H_2}}{P_f}\right)^m e^{-(E_{anode}/RT_f)} \quad (22)$$

$$\frac{1}{R_{cathode}} = k_{cathode}\frac{4F}{RT_a}\left(\frac{p_{O_2}}{P_a}\right)^m e^{-(E_{cathode}/RT_a)} \quad (23)$$

As both electrodes are normally good conductors, a constant cell operating voltage U_{op} throughout the cell is normally considered [1,14].

Some fuel cell performance parameters are defined as follows:

$$\text{Current density}: I = \frac{U_{ocp} - U_{op}}{R_{ohm} + R_{anode} + R_{cathode}} \quad (24)$$

$$\text{Fuel utilization}: U_f = \frac{\bar{I}WL}{2F(4y_{CH_4}^{in} + y_{H_2}^{in} + y_{CO}^{in})F_f^{in}} \quad (25)$$

$$\text{Air utilization}: U_a = \frac{\bar{I}WL}{4Fy_{O_2}^{in}F_a^{in}} \quad (26)$$

$$\text{Power density}: P = \bar{I}U \tag{27}$$

$$\text{Fuel electrical efficiency}: \eta = \frac{P \cdot L \cdot W}{(y^{\text{in}}_{\text{CH}_4}\text{LHV}^{\text{in}}_{\text{CH}_4} + y^{\text{in}}_{\text{H}_2}\text{LHV}^{\text{in}}_{\text{H}_2} + y^{\text{in}}_{\text{CO}}\text{LHV}^{\text{in}}_{\text{CO}})F^{\text{in}}_{\text{f}}} \tag{28}$$

3. SOFC *V–R* mathematical model

3.1. *V–R* characteristic modeling technique

It is difficult to solve partial differential equations. More importantly, the coupling of pressure and flow rate will cause the iteration solution to the equations. Here the volume and resistance (*V–R*) characteristic modeling technique [21] is introduced into the complicated SOFC system modeling to establish ordinary differential equations model. Some state variables were introduced into the model to decouple the pressure and flow rate.

In the fluid system, each component can be treated as one of three types: volume module, resistance module and volume–resistance module. The volume module is the component which can neglect the pressure loss, and accumulate fluid based on the difference of flow rates between the inlet and the outlet. The resistance module is the component where the fluid has an obvious pressure loss, i.e. the pressure of the inlet and outlet is different, which determines the flow rate of the component. To some extent, many fluid components have the qualities of both the volume module and the resistance module. The SOFC system is just this kind of component.

The *V–R* characteristic modeling technique is based on the lumped parameter modeling idea.

In general, the volume module can be described as

$$\frac{\mathrm{d}P}{\mathrm{d}t} = \frac{RT}{\mathrm{dx}}(G_1 - G_2) \tag{29}$$

On the other hand, the resistance module can be described as

$$\frac{\mathrm{d}G}{\mathrm{d}t} = -\frac{A}{\mathrm{dx}}(P_2 - P_1) - \frac{2fG^2}{A\rho d_{\text{h}}} \tag{30}$$

In order to depict the distributed parameter SOFC cell, several control units must be divided in the SOFC, each unit will be treated as a lumped parameter module. In each unit, the module will be separated into two sub-modules. One is a volume sub-module and the other is a resistance sub-module.

Fig. 2 illustrates how the volume–resistance characteristic modeling technique is used in the flow grid. In the conventional modeling method, the pressure and flow rate for the control unit should be solved using iteration method. While in the *V–R* modeling method, the control unit will be divided into two modules. In the volume module, the pressure is considered constant, and the mass flow rate is the state variable. In the resistance module, the mass flow rate is constant, and the pressure is the state variable. Thus, it is no necessary to assume pressure to solve flow rate through iteration algorithm, the pressure and flow rate will be decoupled through two state variables in individual modules.

The key point of the VR model is non-iterative algorithm in the calculation. Therefore, it will save calculation cost, and the most important point is that calculation time can be determined. While for the conventional iteration algorithm, the convergence time cannot be determined owing to the uncertainty of iteration times. The non-iterative algorithm will guarantee VR model to be the real-time model, which can be used in the online simulation.

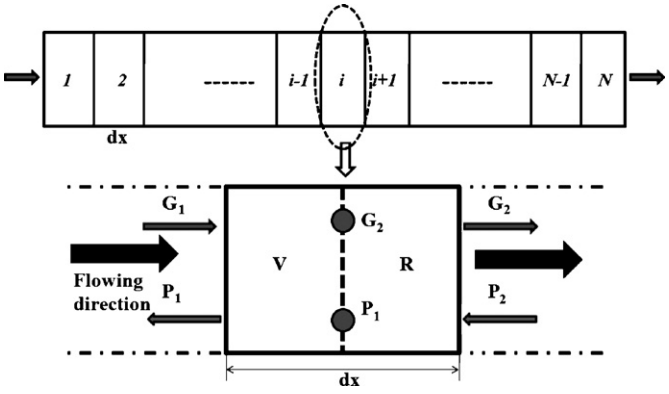

Fig. 2. Diagram of grid mark for mass flow rate and pressure in one section.

3.2. *SOFC V–R characteristic model*

Based on the above idea, one set of equations for the fluid in the control section can be obtained in Table 6.

Here for the gas channels, using the mass balance theorem, the following Eqs. (32) and (36) can be obtained from the volume sub-module; using the momentum balance theorem, the Eqs. (33) and (37) from the resistance sub-module can be obtained. While dealing with the species mass balance and energy balance, the two sub-modules are merged into one control section.

For the solid parts, the energy balance equations of both the PEN structure (12) and the interconnector (13) are considered in one control section.

4. Solution strategy

4.1. *Boundary and initial conditions*

The geometry parameters should be given based on the defined fuel cell stack. All the static variables should be given an initial value to start the simulation, such as molar components, molar flow rates, temperatures of the fuel channel and the air channel as well as the PEN structure and interconnector, etc.

At the same time, boundary condition, i.e. the thermal flux density of both the inlet and the outlet for the solid parts are considered as zero. In addition, the pressure of both channel outlets is given as certain value. As a result, compared with the middle modules, the difference algorithms of both the front and the end modules are different. So the modules at the front and the end are treated independently.

4.2. *Simulation method*

After the conversion from the partial differential equations to the ordinary differential equations based on the

Table 6
SOFC volume–resistance characteristic model

Fuel channel

$$\frac{\mathrm{d}C_{\mathrm{f},i}}{\mathrm{d}t} = -\frac{u_{\mathrm{f},2}C_{\mathrm{f},i,2} - u_{\mathrm{f},1}C_{\mathrm{f},i,1}}{\mathrm{d}x} + \sum_{k\in\{(\mathrm{I}),(\mathrm{II}),(\mathrm{III})\}} v_{i,k}R_{k,2}\frac{1}{h_{\mathrm{f}}}, \quad i\in\{\mathrm{CH_4},\mathrm{H_2},\mathrm{CO},\mathrm{CO_2},\mathrm{H_2O}\} \tag{31}$$

$$\frac{\mathrm{d}G_{\mathrm{f},2}}{\mathrm{d}t} = -A_{\mathrm{f}}\frac{P_{\mathrm{f},2} - P_{\mathrm{f},1}}{\mathrm{d}x} - 2f(W,h_{\mathrm{f}})\cdot\frac{\mu_{\mathrm{f},2}u_{\mathrm{f},2}A_{\mathrm{f}}}{d_{\mathrm{h,f}}^2} \tag{32}$$

$$\frac{\mathrm{d}P_{\mathrm{f},1}}{\mathrm{d}t} = \frac{RT_{\mathrm{f},2}}{M_{\mathrm{f},2}}\left[-\frac{G_{\mathrm{f},2} - G_{f1}}{A_{\mathrm{f}}\mathrm{d}x} - v_{\mathrm{O_2}}R_{\mathrm{O_2},2}M_{\mathrm{O_2}}\frac{1}{h_{\mathrm{f}}}\right] \tag{33}$$

$$\frac{\mathrm{d}T_{\mathrm{f},2}}{\mathrm{d}t} = \frac{\mathrm{d}P_{\mathrm{f},2}}{\mathrm{d}t} - \frac{u_{\mathrm{f},2}T_{\mathrm{f},2} - u_{\mathrm{f},1}T_{\mathrm{f},1}}{\mathrm{d}x} + \frac{1}{\rho_{\mathrm{f},2}C_{\mathrm{p,f},2}h_{\mathrm{f}}}\left[k_{\mathrm{f,PEN},2}(T_{\mathrm{PEN},2} - T_{\mathrm{f},2}) + k_{\mathrm{f,INTC},2}(T_{\mathrm{INTC},2} - T_{\mathrm{f},2}) + \sum_{k\in\{(\mathrm{I}),(\mathrm{II})\}}(-\Delta H)_{k,2}R_{k,2}\right] \tag{34}$$

Air channel

$$\frac{\mathrm{d}C_{\mathrm{a},i}}{\mathrm{d}t} = -\frac{u_{\mathrm{a},2}C_{\mathrm{a},i,2} - u_{\mathrm{a},1}C_{\mathrm{a},i,1}}{\mathrm{d}x} + v_{i,(\mathrm{IV})}R_{(\mathrm{IV})}\frac{1}{h_{\mathrm{a}}}, \quad i\in\{\mathrm{O_2},\mathrm{N_2}\} \tag{35}$$

$$\frac{\mathrm{d}G_{\mathrm{a},2}}{\mathrm{d}t} = -A_{\mathrm{a}}\frac{P_{\mathrm{a},2} - P_{\mathrm{a},1}}{\mathrm{d}x} - 2f(W,h_{\mathrm{a}})\cdot\frac{\mu_{\mathrm{a},2}u_{\mathrm{a},2}A_{\mathrm{a}}}{d_{\mathrm{h,a}}^2} \tag{36}$$

$$\frac{\mathrm{d}P_{\mathrm{a},1}}{\mathrm{d}t} = \frac{RT_{\mathrm{a},2}}{M_{\mathrm{a},2}}\left[-\frac{G_{\mathrm{a},2} - G_{\mathrm{a},1}}{A_{\mathrm{a}}\mathrm{d}x} + v_{\mathrm{O_2}}R_{\mathrm{O_2},2}M_{\mathrm{O_2}}\frac{1}{h_{\mathrm{a}}}\right] \tag{37}$$

$$\frac{\mathrm{d}T_{\mathrm{a},2}}{\mathrm{d}t} = \frac{\mathrm{d}P_{\mathrm{a},2}}{\mathrm{d}t} - \frac{u_{\mathrm{a},2}T_{\mathrm{a},2} - u_{\mathrm{a},1}T_{\mathrm{a},1}}{\mathrm{d}x} + \frac{1}{\rho_{\mathrm{a},2}C_{\mathrm{p,a},2}h_{\mathrm{a}}}[k_{\mathrm{a,PEN},2}(T_{\mathrm{PEN},2} - T_{\mathrm{a},2}) + k_{\mathrm{a,INTC},2}(T_{\mathrm{INTC},2} - T_{\mathrm{a},2})] \tag{38}$$

PEN structure

$$\frac{\mathrm{d}T_{\mathrm{PEN},2}}{\mathrm{d}t} = -\frac{\lambda_{\mathrm{PEN}}}{\rho_{\mathrm{PEN}}C_{p,\mathrm{PEN}}}\times\frac{T_{\mathrm{PEN},3} - 2T_{\mathrm{PEN},2} + T_{\mathrm{PEN},1}}{(\mathrm{d}x)^2} - \frac{1}{\rho_{\mathrm{PEN}}C_{p,\mathrm{PEN}}\tau_{\mathrm{PEN}}}\left\{k_{\mathrm{f,PEN},2}(T_{\mathrm{PEN},2} - T_{\mathrm{f},2}) + k_{\mathrm{a,PEN},2}(T_{\mathrm{PEN},2} - T_{\mathrm{a},2}) - [(-\Delta H)_{(\mathrm{IV}),2}R_{(\mathrm{IV}),2} - I\cdot U] - \left[\frac{\sigma(T_{\mathrm{INTC},2}^4 - T_{\mathrm{PEN},2}^4)}{1/\in_{\mathrm{INTC}} + 1/\in_{\mathrm{PEN}} - 1}\right]\right\} \tag{39}$$

Interconnector

$$\frac{\mathrm{d}T_{\mathrm{INTC},2}}{\mathrm{d}t} = -\frac{\lambda_{\mathrm{INTC}}}{\rho_{\mathrm{INTC}}C_{p,\mathrm{INTC}}}\times\frac{T_{\mathrm{INTC},3} - 2T_{\mathrm{INTC},2} + T_{\mathrm{INTC},1}}{(\mathrm{d}x)^2} - \frac{1}{\rho_{\mathrm{INTC}}C_{p,\mathrm{INTC}}\tau_{\mathrm{INTC}}}\left\{k_{\mathrm{f,INTC},2}(T_{\mathrm{INTC},2} - T_{\mathrm{f},2}) + k_{\mathrm{a,INTC},2}(T_{\mathrm{INTC},2} - T_{\mathrm{a},2}) - \left[\frac{\sigma(T_{\mathrm{INTC},2}^4 - T_{\mathrm{PEN},2}^4)}{1/\in_{\mathrm{INTC}} + 1/\in_{\mathrm{PEN}} - 1}\right]\right\} \tag{40}$$

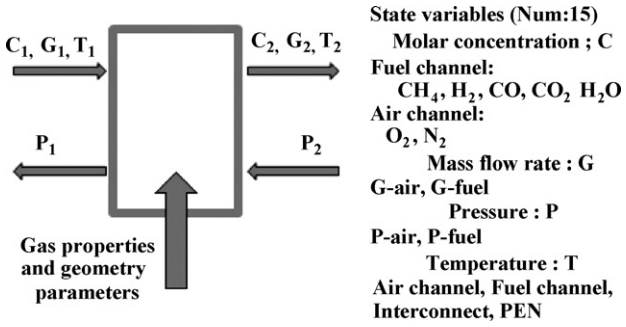

Fig. 3. Flowing interface of the control section in SOFC cell.

distributed–lumped parameter method and the volume–resistance characteristic modeling technique, the single module of every unit is given in Fig. 3.

The system model, which is based on the above mathematical model, was developed on the EASY5 simulation platform using the FORTRAN language compiler.

5. Result and discussion

In this section, a specific co-flow fuel cell is simulated. Section 5.1 introduces the model input parameters and operating conditions; Section 5.2 analyzes the steady-state performance of a co-flow SOFC system; Section 5.3 briefly studies a transient process with a step change.

5.1. Input parameters and operating conditions

The geometry input parameters and some other physical and electrical properties adopt the parameters in Ref. [1]. The main geometry dimension parameters and operating conditions are listed in Table 7.

Table 7
Key geometry parameters and operating conditions

Dimension parameters (unit: m)	
Cell length	0.4
Cell width	0.1
Fuel channel height	0.001
Air channel height	0.001
Anode thickness	5E−4
Cathode thickness	5E−5
Electrolyte thickness	2E−5
Interconnector thickness	5E−4
Operating conditions	
Inlet fuel and air temperature	1173 K
Outlet fuel and air pressure	1.0 bar
Inlet fuel molar flow rate	0.0012 mol s^{-1}
Inlet air molar flow rate	0.012 mol s^{-1}
Fuel composition	0.1710 CH_4, 0.2626 H_2, 0.0294 CO, 0.0436 CO_2, 0.4934 H_2O
Air composition	0.21 O_2, 0.79 N_2
Fuel utilization	0.85

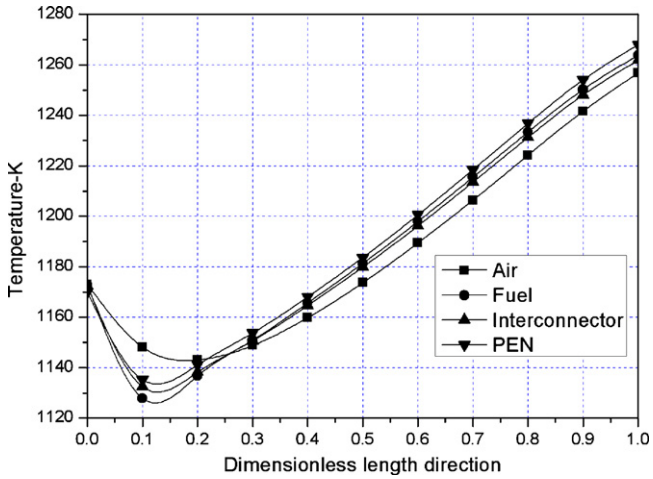

Fig. 4. Fuel and air channels, interconnector and PEN structure temperature profiles along the cell length.

5.2. Steady-state simulation results

The steady-state simulation is based on the above input parameters and operating conditions.

The temperature profiles of the fuel and air channels, the interconnector and PEN structure along the cell length are presented in Fig. 4. Owing to the endothermic reaction of the reforming of methane at the entrance, the temperature decreases by 50 K. Then the temperature increases along the fuel and air flow directions by heat accumulation, which is released by the electrochemical and water gas shift reactions. The maximum temperature occurs at the outlet. In general, the maximum tolerable temperature gradient is approximately 10 K cm^{-1} by assuming a maximum safe stress-induced strain of 0.1% and a thermal expansion coefficient for the YSZ material [13]. Thus, the temperature gradient calculated for the base case is reasonable.

In this type of fuel cell stack, internal reforming reaction, the water gas shift reaction and the electrochemical reaction will occur simultaneously. The mole fraction profiles along the cell length of all the species in the fuel channel steam are illustrated in Fig. 5. Methane will be reformed rapidly at the entrance of the fuel cell. Consequently, the concentration of the hydrogen increases fast. Then the electrochemical reaction displays the main influence, the hydrogen concentration will decrease along the cell, the carbon dioxide will increase correspondingly. For the rated case, at the exit of the fuel channel, all the methane has been fully consumed, and the composition is 7.97% in H_2, 2.93% in CO, 15.25% in CO_2, 73.84% in H_2O.

Figs. 6 and 7 present the profiles of the dimensionless gas properties (pressure, velocity, density, specific heat capacity, thermal conductivity and dynamic viscosity) along the cell length in the air and fuel channel, respectively. The dimensionless gas properties are defined to be the ratio of local values and corresponding inlet gas properties parameters. The inlet gas properties can be calculated by the inlet conditions using the methods depicted in Refs. [22,23]. It is clearly shown that the variation of the gas properties is lower in the air channel than in the fuel channel [3].

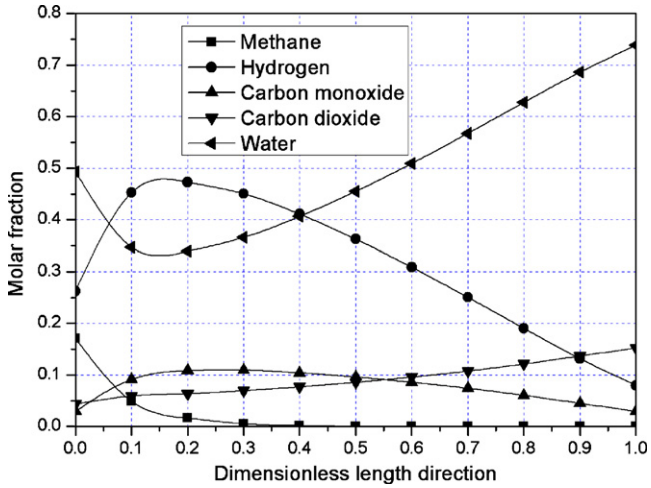

Fig. 5. Fuel channel component mole fractions profiles along the cell length.

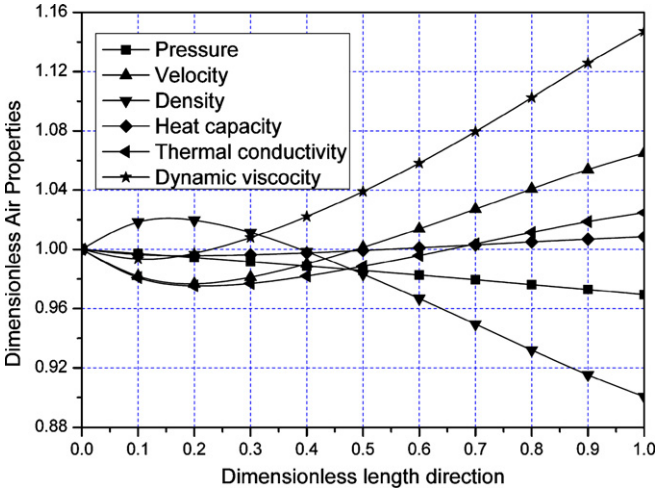

Fig. 6. Air channel dimensionless property profiles along the cell length.

The pressure drops by 3.06% and 0.12% in the air and fuel channels, respectively. In general, the flow rate and temperature will increase along the cell length in the fuel channel. So the pressure should increase if the flow resistance is not considered.

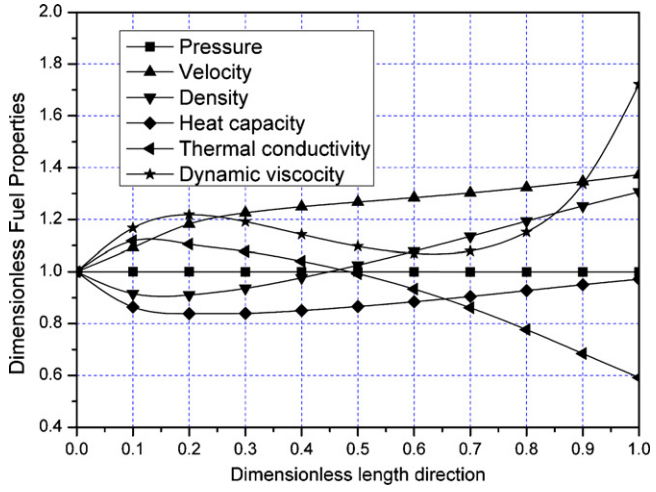

Fig. 7. Fuel channel dimensionless property profiles along the cell length.

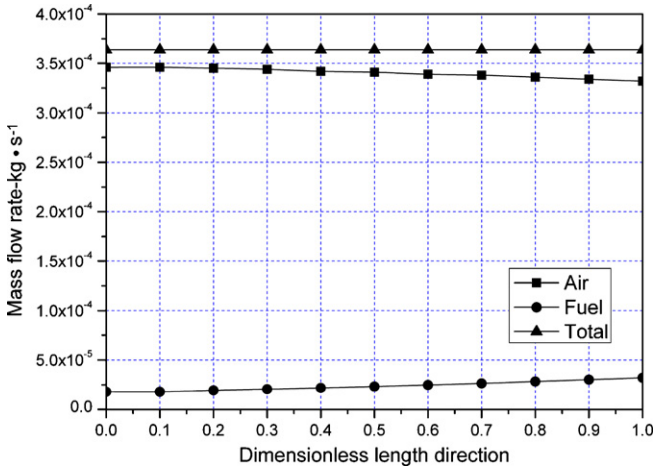

Fig. 8. Mass flow rate profiles along the cell length.

Here, owing to the increasing of the velocity, the pressure loss will increase along the cell length. Therefore, the pressure drop due to flow resistance will be dominated, and this causes the pressure drop in the fuel channel.

The density is related to the pressure and the temperature based on the gas state equation. In the air channel, the pressure has little change at the entrance, while the temperature drops, so the density in the air channel will rise at the entrance. With the increase of the temperature along the cell length, the density will drop. In the fuel channel, the result can be obtained based on the same analysis.

Velocity is influenced by both the mass flow rate and density. Owing to the increase of density at the entrance, the velocity in the air channel will drop. With the decrease of density, the mass flow rate changes a little, so the velocity will increase along the cell length. While the velocity in the fuel channel always rises along the cell length, this is mainly influenced by the increasing mass flow rate.

Other gas properties, such as specific heat capacity, thermal conductivity and dynamic viscosity, are primarily influenced by the temperature and the gas composition. This has been discussed by the author Todd and Young [22]. All the profiles of relevant gas properties are consistent with Ref. [3].

As the oxygen ions transfer from the air channel to the fuel channel, the mass flow rate decreases in the air channel, while increases in the fuel channel along the cell. Fig. 8 illustrates the distribution of mass flow rate in both the air and fuel channels. The total mass in the fuel cell is also provided to prove that the VR model accurately satisfy the mass conservation.

Fig. 9 illustrates the individual contribution of various potential losses, as well as the current density along the cell length. The potential losses and current density distribution are related to the composition of the gas steam and the temperature along the cell. For high-temperature SOFC, the ohmic activation loss is only of small portion, while the cathode and anode activation losses are the predominant source of losses. Along the cell length, the open circuit voltage and cathode activation loss have the same trend. It increases near the entrance and decreases near the exit, while the anode activation loss is almost constant. Thus,

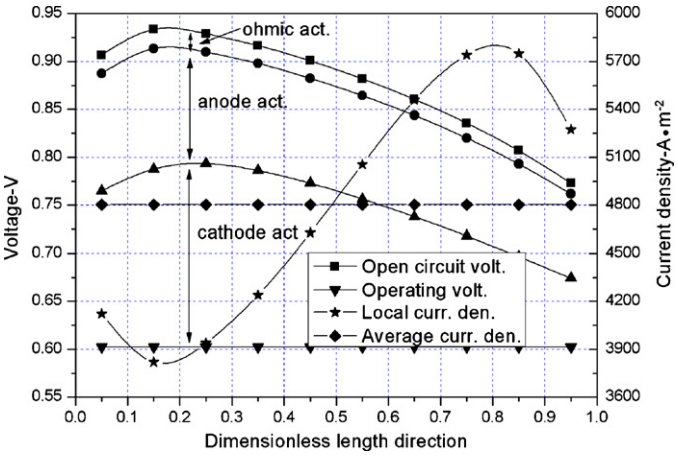

Fig. 9. Contribution of various potential losses and current density along the cell length.

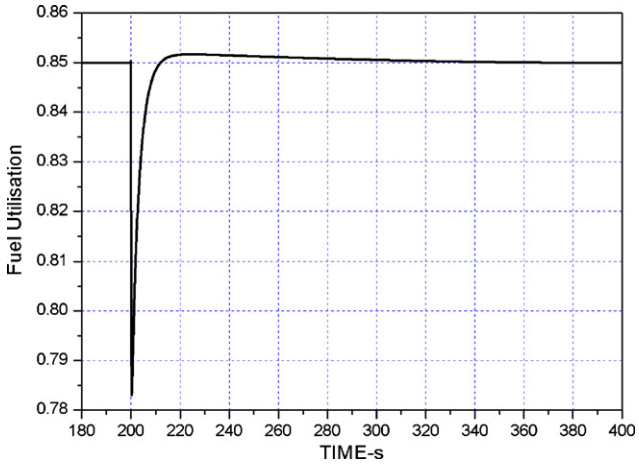

Fig. 10. Dynamic response of fuel utilization.

improving the operating temperature can effectively decrease the cathode activation loss. The current density is a complicated physical property, which is concerned with PEN temperature, partial pressure of fuel and fuel utilization, etc. [2]. It decreases at the entrance due to the decreasing of PEN temperature. With the increasing of PEN temperature, it will rise in the center of fuel cell. At the exit, the current density will decrease owing to the lower partial pressure of fuel.

The simulation result above is consistent with Refs. [1–3,10,12,17,18,24], which verifies that the model established in this study is useful and feasible. For the rated case, the predicted values are as following: the operating voltage is 0.603 V; the average current density is 4802.7 A m^{-2}; the power density is 2892.7 W m^{-2}; the fuel electrical efficiency is 46.1%.

5.3. Dynamic simulation results

In this section, the transient behavior of the fuel cell is investigated. Based on the above basic steady-state case, a fuel molar rate step changes 10% is imposed on the fuel channel when the fuel cell system has operated for 200 s. Figs. 10–12 presents the dynamic response of the fuel cell performance.

Fuel utilization is a very important performance parameter, because it will determine whether or not the whole system is stably operating. Here, PID control technique is adopted to keep the fuel utilization constant through adjusting the operating voltage. The definition of the fuel utilization is presented in formula (25). Fig. 10 gives the response of fuel utilization. When fuel molar flow rate is increased suddenly, first the consumed fuel cannot change at the moment, so fuel utilization has a sharp drop at the time 200 s. Thus, the operating voltage decreases fast, and the current density will increase correspondingly. The temperature of the PEN structure will also increase due to the electrochemical reaction with the increasing consumed fuel. Finally fuel utilization will be back to the constant 0.85 owing to the PID controller.

Fig. 11 presents the dynamic response of the performances of the fuel cell. When the fuel molar rate is increased, the predicted operating voltage will drop to 0.583 V, average current density will increase to 5282.9 A m^{-2}, power density will increase to 3078.3 W m^{-2}, but fuel electrical efficiency will decrease to 44.6%.

Fig. 12 presents the dynamic response of the temperatures at the exit of the fuel and air channels, interconnector and PEN

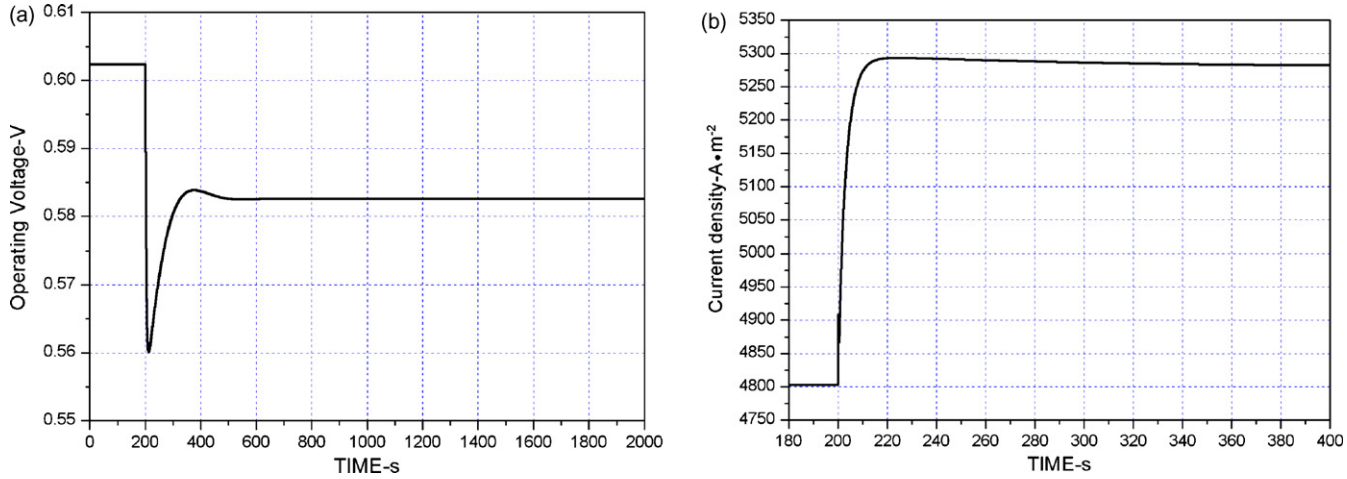

Fig. 11. (a) Dynamic response of operating voltage of fuel cell. (b) Dynamic response of average current density of fuel cell.

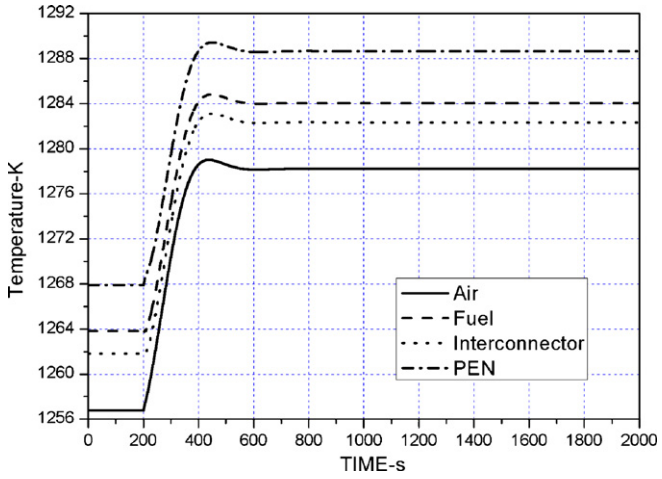

Fig. 12. Temperature dynamic response of fuel and air channel, interconnect and PEN at the exit.

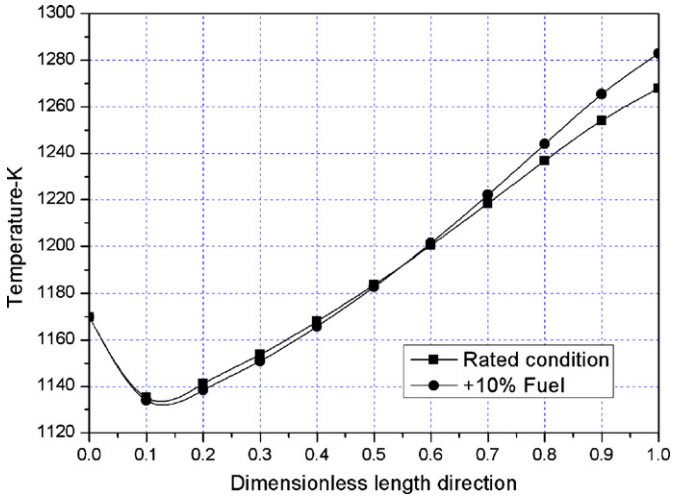

Fig. 13. PEN structure temperature profile comparison along the cell length.

structure. As can be seen, the temperature will increase when the fuel molar rate is increased. The maximal PEN structure temperature will increase to 1284 K.

According to Figs. 11 and 12, the inertia delay time of temperature and operating voltage is about 500 s which is mainly explainable in term of the fuel cell great thermal capacity. But the inertia delay time of current density is only about 160 s. This result can be useful and meaningful for the design of the control system.

In some sense, increasing the fuel flow rate will improve the performance of the fuel cell, but some problems should be considered carefully, such as larger gradient in temperature (Fig. 13) and current density (Fig. 14). Therefore, the operation of system regulation should be appropriate and cautious.

6. Conclusions

This paper developed the mathematical model of DIR-SOFC, successfully introduced the volume–resistance characteristic modeling technique into the SOFC modeling. Based on this *V–R* modeling technique, the distributed–lumped parameter method

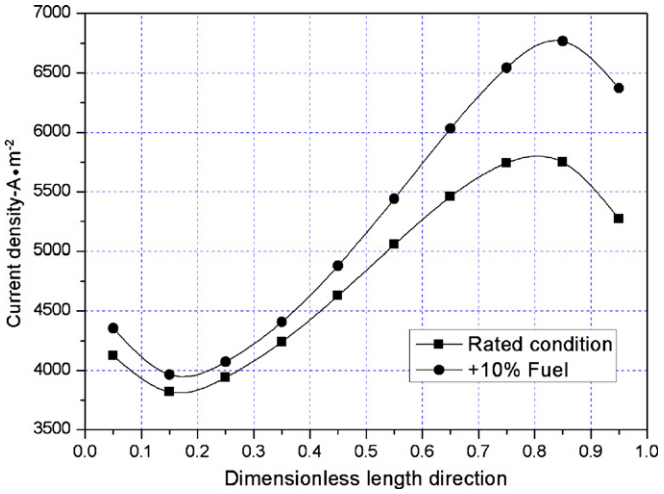

Fig. 14. Current density distribution comparison along the cell length.

and the modular modeling idea, the distributed parameter SOFC simulation model was established. This non-iterative model can satisfy the requirement of the quick dynamic and real-time simulation.

This model can predict the fuel cell distribution properties, such as the temperature, fuel compositions, current density, voltage losses, etc. The detailed local gas properties is also considered along the cell length, such as pressure, mass flow rate, velocity, density, dynamic viscosity, thermal conductivity and heat capacity, etc. It is valuable and meaningful for the design and optimization of the fuel cell system.

SOFC system has great thermal capacity indeed, but current density delay time is very short, only about 160 s. Dynamic simulation could provide reference for the control system research and design in future.

Acknowledgement

This project was supported by National Natural Science Foundation of China (NSFC) under the contract no. 50676061.

References

[1] P. Aguiar, C.S. Adjiman, N.P. Brandon, J. Power Sources 138 (2004) 120–136.
[2] EG&G Technical Services Inc., Fuel Cell Handbook, 7th ed., U. S. Department of Energy Office of Fossil Energy National Energy Technology Laboratory, 2004.
[3] P. Iora, P. Aguiar, C.S. Adjiman, N.P. Brandon, Chem. Eng. Sci. 60 (2005) 2963–2975.
[4] C. Stiller, Design, Operation and Control Modeling of SOFC/GT Hybrid Systems, PhD Thesis, Trondheim, 2006.
[5] E. Achenbach, E. Riensche, J. Power Sources 52 (1994) 283–288.
[6] E. Achenbach, J. Power Sources 49 (1994) 338–348.
[7] S. Campanari, P. Iora, Fuel Cell 5 (1) (2005) 34–51.
[8] S. Campanari, P. Iora, J. Power Sources 132 (2004) 113–126.
[9] H. Yakabe, T. Sakurai, Solid State Ionics 174 (2004) 295–302.
[10] A. Lazzaretto, A. Toffolo, J. Energy Resour. Technol. 126 (2004) 40–46.
[11] N. Bessette, Modeling and Simulation for Solid Oxide Fuel Cell Power Systems, PhD Thesis, Georgia Institute of Technology, Atlanata, 1994.
[12] M. Pfafferodt, P. Heidebrecht, M. Stelter, J. Power Sources 149 (2005) 53–62.

[13] L.T. Lim, D. Chadwich, L. Kershenbam, Ind. Eng. Chem. Res. 44 (2005) 9609–9618.
[14] P. Aguiar, D. Chadwick, L. Kershenbaum, Chem. Eng. Sci. 57 (2002) 16665–21677.
[15] C. Stiller, B. Thorud, S. Seljebo, et al., J. Power Sources 141 (2005) 227–240.
[16] P. Costamagna, A. Selimovic, M.D. Borghi, et al., J. Chem. Eng. 102 (2004) 61–69.
[17] R. Bove, P. Lunghi, N.M. Sammes, J. Hydrogen Energy 30 (2005) 181–187.
[18] P. Costamagna, L. Magistri, A.F. Massardo, J. Power Sources 141 (2001) 352–368.
[19] V.M. Janardhanan, O. Deutschmann, J. Power Sources 162 (2006) 1192–1202.
[20] H.-C. Liu, C.-H. Lee, Y.-H. Shiu, et al., J. Power Sources 167 (2007) 406–412.
[21] H. Zhang, S. Weng, M. Su, ASME TURBO EXPO, 2005-68293.
[22] B. Todd, J.B. Young, J. Power Sources 110 (2002) 186–200.
[23] B.E. Poling, J.M. Prausnnitz, J.P. O'Connell, The Properties of Liquids & Gases, 5th ed., McGraw-Hill, New York, 2000.
[24] J.P.P. Huijsmans, Curr. Opin. Solid State Mater. Sci. 5 (2001) 317–323.
[25] J.M. Smith, H.C. Van Ness, M.M. Abbott, Introduction to Chemical Engineering Thermodynamics, 7th ed., McGraw-Hill, New York, 2005, pp. 140–141.